JACS
JOURNAL OF THE AMERICAN CHEMICAL SOCIETY
Communication
pubs.acs.org/JACS

Synthesis, Alignment, and Magnetic Properties of Monodisperse Nickel Nanocubes

Alec P. LaGrow,[†] Bridget Ingham,[‡] Soshan Cheong,[†,‡] Grant V. M. Williams,[†,‡] Christian Dotzler,[‡,#] Michael F. Toney,[#] David A. Jefferson,[§] Elena C. Corbos,[⊥] Peter T. Bishop,[⊥] James Cookson,[⊥] and Richard D. Tilley*[,†,‡]

[†]School of Chemical and Physical Sciences and the MacDiarmid Institute for Advanced Materials and Nanotechnology, Victoria University of Wellington, Wellington 6012, New Zealand

[‡]Industrial Research Limited and MacDiarmid Institute, P.O. Box 31-310, Lower Hutt 5040, New Zealand

[#]Stanford Synchrotron Radiation Lightsource, SLAC National Accelerator Laboratory, Menlo Park, California 94025, United States

[§]The University Chemical Laboratories, Cambridge University, Lensfield Road, Cambridge CB2 1EW, U.K.

[⊥]Johnson Matthey Technology Centre, Blount's Court, Sonning Common, Reading RG4 9NH, U.K.

Supporting Information

ABSTRACT: This Communication describes the synthesis of highly monodispersed 12 nm nickel nanocubes. The cubic shape was achieved by using trioctylphosphine and hexadecylamine surfactants under a reducing hydrogen atmosphere to favor thermodynamic growth and the stabilization of {100} facets. Varying the metal precursor to trioctylphosphine ratio was found to alter the nanoparticle size and shape from 5 nm spherical nanoparticles to 12 nm nanocubes. High-resolution transmission electron microscopy showed that the nanocubes are protected from further oxidation by a 1 nm NiO shell. Synchrotron-based X-ray diffraction techniques showed the nickel nanocubes order into [100] aligned arrays. Magnetic studies showed the nickel nanocubes have over 4 times enhancement in magnetic saturation compared to spherical superparamagnetic nickel nanoparticles.

Nickel nanoparticles have received a great deal of interest due to their unique magnetic and catalytic properties,[1] and they have been used in applications such as catalysis,[1,2] magnetics,[3,4] and bioseparation.[3] Superparamagnetic nickel has been studied for magnetically recyclable catalysts[4] and histidine-tagged protein separation,[3] as its particles do not magnetically aggregate in solution without an external magnetic field.[3,4] However, spherical nickel nanoparticles in the superparamagnetic regime have been reported to have greatly decreased magnetic saturation at room temperature compared with the bulk nickel.[1,3,5,6] Nickel nanoparticles smaller than 15 nm are typically superparamagnetic, with magnetic saturations of less than 2% of the bulk value.[1,3,5,6] Higher magnetic saturation can be achieved for larger nickel particle sizes,[5] although this also increases the blocking temperature to near room temperature, with the particles becoming ferromagnetic.[5] The resulting change of magnetic properties is reported to be due to the particles being partially amorphous,[5] as well as oxidation of the nickel.[1] To circumvent this, syntheses that form superparamagnetic, highly crystalline, single-domain nickel nanoparticles are highly desirable.

Nickel adopts the face-centered cubic (fcc) crystal structure, which enables cuboctahedral, icosahedral, and cubic shapes to form.[7] Of these shapes, nanocubes are of interest for catalytic applications, as they exhibit only the {100} facet on their surface.[8] For magnetic applications monodisperse nanocubes can orient into arrays with 100% packing density and the crystal lattice on every cube is oriented in the same direction.[9] However, small (<15 nm), highly monodisperse metallic nanocubes have only been formed for palladium,[10] rhodium,[11] iron,[12] and platinum.[13−15] This difficulty in forming nanocubes compared to cuboctahedra or icosahedra is due to the higher energy of the {100} faces compared to {111} faces for very small fcc nanocrystals.[7] Recent syntheses with platinum and iron have successfully formed nanocubes by stabilizing the {100} facets during reduction of precursors by either hydrogen gas[12,13] or carbon monoxide,[14,16,17] with surfactant molecules to aid the shape control.[12−14,16,17] From computational work studying the synthetic formation mechanism of platinum nanocubes, it was found that the combination of both the carbon monoxide and amine adsorbed to the surface of the platinum makes the {100} face the lowest energy facet, which then favors the formation of nanocubes.[17]

Spherical nickel nanoparticles are commonly synthesized via the decomposition of nickel acetylacetonate [$Ni(acac)_2$]. The nanoparticle size can be controlled by altering the surfactant to nickel ratio and the type of amine and phosphine surfactants.[1,5] Besides spheres, so far there are only a few limited examples of nickel nanocrystals shapes in the literature, with only rods,[8] triangular[19,20] and hexagonal plates[20] reported. Among these, hydrogen gas has been utilized in combination with surfactants such as glycolate for the formation of triangular plates,[19] and amines in the formation of rods.[18]

Herein we report the synthesis of monodisperse 12 nm nickel nanocubes via the reduction of $Ni(acac)_2$ under mild hydrogen pressure. The hydrogen and the surfactants hexadecylamine (HDA) and trioctylphosphine (TOP) are used to favor the

Received: October 31, 2011
Published: December 23, 2011

dx.doi.org/10.1021/ja210209r | J. Am. Chem.Soc. 2012, 134, 855−858

cubic morphology. TOP is also used to tailor the nanoparticle size, at lower ratios of TOP to nickel, nanocubes are formed and at higher ratios smaller spherical 5 nm nanoparticles are produced. The 12 nm nanocubes are superparamagnetic and have over 4 times the magnetic saturation of both our 5 nm spherical nickel nanoparticles and values typically reported for superparamagnetic nickel nanocrystals.[1,3,5,6]

In a typical synthesis, $Ni(acac)_2$ was dissolved in mesitylene, added with 10 mol equiv of HDA and 0.5 mol equiv of TOP to the metal precursor. The precursor solution was reacted at 140 °C in 1 bar hydrogen in a closed reaction vessel.[21−24] After cooling to room temperature, the nanoparticles were purified in ambient conditions open to the air by attracting them to a magnet and removing the solution. The nanoparticles were redispersed in toluene and the purification step was repeated twice.

The transmission electron microscopy (TEM) image of the sample in Figure 1A shows nanocubes with an average edge

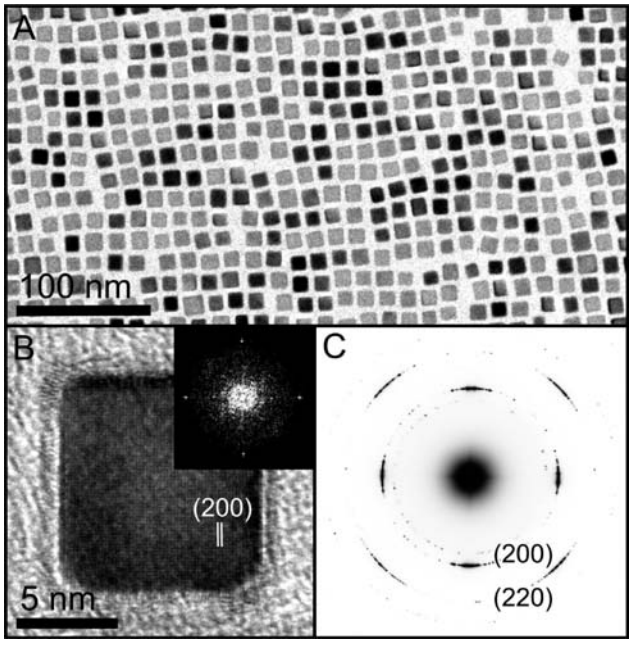

Figure 1. (A) TEM image of an array of nickel nanocubes. (B) HRTEM image of a nickel nanocube, with an inset of the FFT. (C) Electron diffraction of (A) indexed to {200} and {220} planes of fcc nickel. The faint inner ring is nickel {111} due to a small amount of misoriented nanocubes.

length of 12 nm (11.6 ± 0.8 nm) assembling into periodic arrays across the TEM grid, indicating a high degree of monodispersity. The nanocube sample contained 57% of cubes with an aspect ratio of 1.0, 38% have an aspect ratio of 1.1, and 5% have an aspect ratio of 1.2. Figure 1B shows the high-resolution (HR) TEM image of a typical single nanocube. Each nanocube has lighter contrast around the edge and this shell is 1 nm (1.0 ± 0.2 nm) thick. As can be seen in Figure 1B the nanocubes have a single crystalline core with lattice fringes that correspond to the (200) spacing of nickel. The fast Fourier transform (FFT) of the single nanocube image (Figure 1B inset) has a four-fold symmetry between the points matching the four {200} reflections of the fcc structure viewed down a ⟨100⟩ zone axis. The electron diffraction of the assembly in Figure 1A is shown in Figure 1C and has the same four-fold symmetry of the {200} and {220} reflections indicating that the nanocubes assemble into ⟨100⟩ oriented arrays.

A HRTEM image of a nanocube and shell is shown in Figure 2A. Two sets of lattice fringes from the shell had

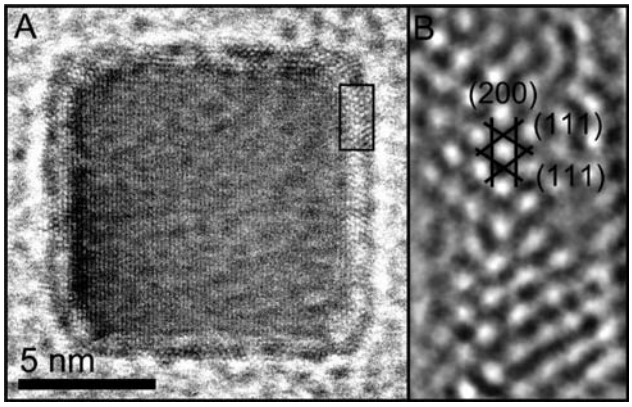

Figure 2. (A) HRTEM image of a nickel nanocube. (B) High magnification of boxed area in (A) with NiO planes indexed.

spacings of 2.40 Å and at an angle of 70° to each other, another set of fringes had spacings of 2.10 Å (Figure 2 B). These match nickel oxide (NiO) down the [110] zone axis. The {200} planes of the nickel oxide shell are also parallel to the {200} planes of the nickel core (Figure 2A). The oxide layer is formed when the reaction vessel is opened to air and during the purification process as previously observed with iron nanoparticles.[24,25] A powdered sample of the nanocubes and a sample left as adispersion in toluene were examined in the TEM after 6 months. As can be seen in the images in Figures S1 and S2, no noticeable increase in shell thickness occurred, indicating that the nanocubes are stable to further oxidation.

Synchrotron X-ray diffraction (XRD) measurements were performed on nickel nanocubes dried on a silicon substrate. The XRD pattern of the nanocubes shows diffraction peaks of fcc nickel with no other phases present (Figure 3). The 1 nm

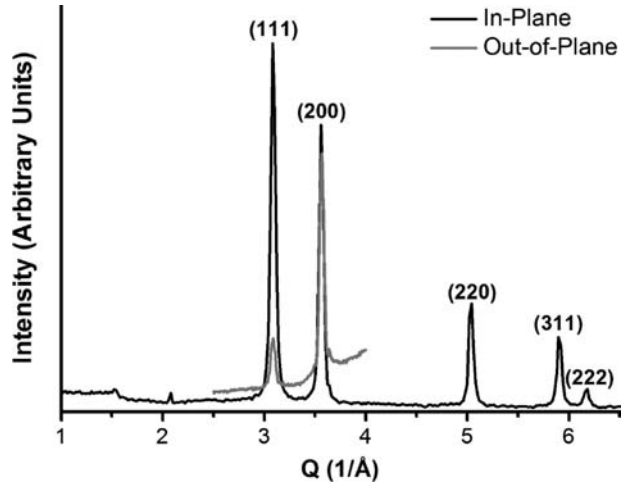

Figure 3. In-plane and out-of-plane synchrotron XRD scans of the nickel nanocubes dried on a silicon substrate.

oxide shell is most likely too thin to give a clear signal. Using the Scherrer equation the crystallite size is calculated as 10.0 ± 0.2 nm. Small angle X-ray scattering (SAXS) data suggest that most of the sample is of cubic shape with an average edge

dx.doi.org/10.1021/ja210209r | J. Am. Chem.Soc. 2012, 134, 855−858

length of 11 nm (Figure S3). The SAXS and XRD data are in agreement with the TEM data, indicating that the particles are single crystalline and that the monodisperse nanocubes observed in the TEM are representative of the product.

To investigate possible preferential orientation in the arrangement of the nanocubes, in-plane, out-of-plane, and rocking scans (partial pole figures) for selected reflections were carried out (see Figures S4–S9). In the out-of-plane scan, the (200) peak area is 4 times larger than that of the (111) peak (Figure 3). In a nickel sample without any preferential orientation the (200) peak area would be expected to be approximately 45% of the (111) peak. Similarly for the in-plane measurement, the (200) peak area is 72% of the (111) peak (Figure 3). The enhanced (200) peak area is due to the preferential [100] alignment of the nickel nanocubes. This is further confirmed by the (200) rocking scans, which show intensity maxima at orientation angles expected for this preferential alignment (Figure S6 and S7). The orientation effects in the XRD experiments agree with the TEM observation that the nanocubes assemble into [100] aligned arrays.

Nanoparticle size and shape were found to be strongly influenced by small additions of the surfactant TOP. In a series of experiments, the amount of the HDA surfactant was kept constant at 10 mol equiv to the $Ni(acac)_2$. In the absence of TOP, polydisperse and irregularly shaped nanoparticles of 30 ± 11 nm in size were formed, as shown in Figures 4A and S10A. With the addition of 0.5 and 1 mol equiv of TOP, highly monodisperse nanoparticles were obtained, as shown in Figures 4B,C and S10B,C. Nanocubes of 11.6 ± 0.8 nm (Figure 4B) and spherical nanoparticles of 5.1 ± 0.7 nm (Figure 4C) were formed with 0.5 and 1 mol equiv of TOP, respectively. These results show that adding relatively small amounts of TOP can successfully control both the size and monodispersity of the nickel nanoparticles, which is consistent with other reports.[3,5]

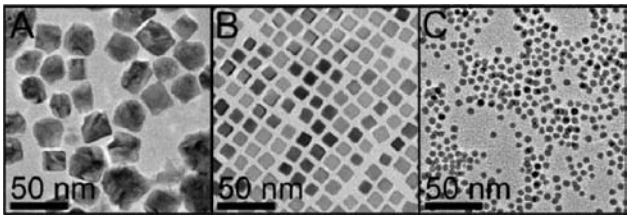

Figure 4. TEM images of the nickel nanoparticles synthesized with 10 mol equiv HDA and varying the ratio of TOP of (A) 0 mol equiv, (B) 0.5 mol equiv and (C) 1 mol equiv

To date, the formation of nickel cubes below 15 nm has not been achieved. In most reactions forming nickel, such as the hot injection method, nucleation and growth happen in minutes.[1] During the synthesis reported here the nickel nanocubes the take 24 h to fully grow. After a reaction time of 4 h, 8.2 ± 1.3 nm polyhedral seeds form; after 12 h, the seeds have grown into nanocubes with an average edge length of 9.3 ± 1.1 nm; and after 24 h and longer, the nanocubes are 11.6 ± 0.8 nm in size (Figure S11). The long reaction time means that there is slow growth of the nanoparticles allowing for the atoms to move to thermodynamically favorable positions. For fcc metals the most thermodynamically stable shape for nuclei and single crystal particles is the cuboctaherdra bound by {111} and {100} facets.[7] In this reaction nanocubes are formed indicating that the {100} faces are the thermodynamically most stable in these reaction conditions. In this system hydrogen gas, phosphine and amine surfactants are all necessary to favor nanocube formation. Of these, the hydrogen and TOP are expected to bind most strongly to the nanocrystal surfaces. The main role of the TOP is most likely in controlling the nanocrystal size, with no evidence of stronger faceting at higher (1 equiv) TOP concentrations in Figure 4C. Theoretical work on the bonding of hydrogen to different nickel crystal faces has shown that the bridging site on the {100} face of nickel is the most energetically stable for hydrogen to occupy and this could stabilize the {100} face of the nickel nanocubes in our system.[26] This result is in agreement with previous reports of reducing gases such as CO combined with surfactants stabilizing the {100} faces of fcc metals such as 10 nm platinum cubes.[17] The cubic shape was not favored for the 5.1 nm spherical nickel nanoparticles shown in Figure 4C. This is most likely due to the partially amorphous nature of these nanoparticles compared to the highly crystalline nanocubes.

Magnetic measurements were carried out on the nanocubes. As shown in Figure 5, the magnetization curve at 300 K intercepts at the origin, with both remnant magnetization and coercivity absent, indicating that the nanocubes are superparamagnetic. The blocking temperature was 97.5 K at 33 Hz (Figure S12). At 10 K, the nanocubes are ferromagnetic showing hysteresis with a coercivity of 105 Oe and a remnant magnetization of 3.2 emu/g Ni (Figure 5 inset). From the hysteresis loops the saturated magnetization values at 60 kOe are 10.0 and 12.4 emu/g Ni at 300 and 10 K, respectively (Figure 5). These compare to the value of bulk nickel of 55emu/g at 300 K.[27] Similar magnetic measurements were performed on the 5.1 nm spherical nickel nanoparticles and the magnetization curve is shown in Figure S13. At 300 K the nickel nanospheres were superparamagnetic with a magnetic response of 2.3 emu/g Ni at 60 kOe. At 10 K the nanoparticles had ferromagnetic hysteresis, with a magnetic response of 19.2 emu/g Ni at 60 kOe.

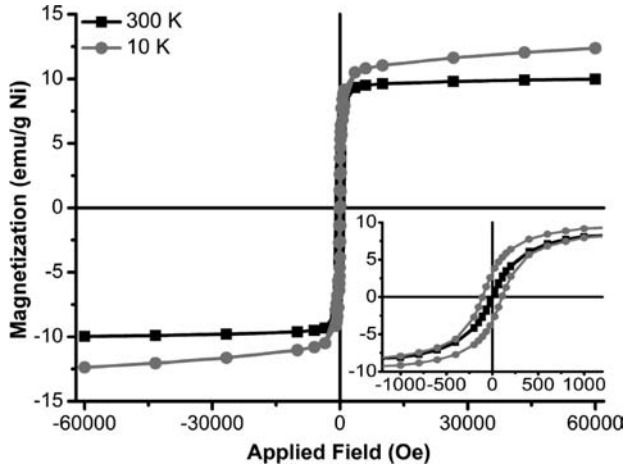

Figure 5. Magnetization curves at 10 and 300 K for the nickel nanocubes and inset of the hysteresis behavior.

The 300 K magnetic saturation of the 11.6 nm nickel nanocubes is over 4 times that of the 5.1 nm spherical nanoparticles and over 10 times that of similarly sized 11–13 nm, superparamagnetic, spherical nickel nanoparticles, previously reported that typically have values below 1.0 emu/g.[3,5,6] Mezailles et al. proposed that their 12 nm nickel nanoparticles were paramagnetic due to low crystallinity.[5] In comparison, the superparamagnetic nanocubes reported here are highly crystalline,

dx.doi.org/10.1021/ja210209r | J. Am. Chem.Soc. 2012, 134, 855–858

and this could explain the increase in magnetization saturation.[3,5,6] The over 10 times increase in magnetic properties makes the nanocubes ideal for separation of histidine-tagged proteins[3] and magnetically recyclable catalysts.[4]

The 1 nm crystalline NiO shell around the nickel core can potentially lead to an exchange bias because bulk NiO is antiferromagnetic with a Néel temperature of 525 K and bulk fcc nickel is ferromagnetic with a Curie temperature of 631 K.[27,28] The exchange bias can lead to a shift in the magnetization loops away from the origin when cooled in an applied magnetic field. To check for this possibility, the sample was cooled in an applied magnetic field of 50 000 Oe down to 10 K. No detectable shift in the magnetization loop was observed when compared with zero field cooled data. This is consistent with experimental results reported by Tracy et al. that NiO shells below 2 nm can be too small to exhibit an exchange shift.[29]

In summary, monodisperse 12 nm nickel nanocubes and 5 nm monodisperse nanospheres have been synthesized by reducing $Ni(acac)_2$ in a hydrogen environment with HDA and TOP as surfactants. The nanoparticle size is controlled by the TOP to Ni precursor ratio and leads to a monodisperse product. The nanocubes shape is controlled by thermodynamic growth with the hydrogen and TOP favoring the {100} facets. The nanocubes order into [100] aligned assemblies when deposited as a monolayer into [100] aligned assemblies. The nanocubes are superparamagnetic at room temperature and have a magnetic saturation of 10.0 emu/g Ni, which is over 10 times higher than previously reported spherical nanoparticles of the same size range.[3,5,6] The nanocubes magnetic behavior of these nickel nanocubes makes them ideal for applications in bioseparation and as magnetically recyclable catalysts.

■ ASSOCIATED CONTENT

Supporting Information

Experimental details for synthesis, TEM, SQUID, additional information on particle size distributions, and synchrotron XRD and SAXS experimental methods and results. This material is available free of charge via the Internet at http://pubs.acs.org.

■ AUTHOR INFORMATION

Corresponding Author

richard.tilley@vuw.ac.nz

■ ACKNOWLEDGMENTS

A.P.L. thanks Victoria University for funding. R.D.T. and S.C. thank the MacDiarmid Institute and MSI for funding through grant PROJ-13733-NMTS and CONT-20707-NMTS-IRL. E.C.C. thanks the European Commission for a fellowship (PIIF-GA-2009-252242: NANOTUNE). Portions of this research were carried out at the Stanford Synchrotron Radiation Lightsource, a national user facility operated by Stanford University on behalf of the U.S. Department of Energy, Office of Basic Energy Sciences. SAXS experiments were undertaken at the Diamond Light Source (Experiment SM-6687-1).

■ REFERENCES

(1) Park, J.; Kang, E.; Son, S. U.; Park, H. M.; Lee, M. K.; Kim, J.; Kim, K. W.; Noh, H.-J.; Park, J.-H.; Bae, C. J.; Park, J.-G.; Hyeon, T. *Adv. Mater.* **2005**, *17*, 429.

(2) Metin, Ö.; Mazumder, V.; Özkar, S.; Sun, S. *J. Am. Chem. Soc.* **2010**, *132*, 1468.

(3) Lee, I. S.; Lee, N.; Park, J.; Kim, B. H.; Yi, Y. W.; Kim, T.; Kim, T. K.; Lee, I. H.; Paik, S. R.; Hyeon, T. *J. Am. Chem. Soc.* **2006**, *128*, 10658.

(4) Guo, H.; Chen, Y.; Chen, X.; Wen, R.; Yue, G.-H.; Peng, D.-L. *Nanotechnology* **2011**, *22*, 195604.

(5) Carenco, S.; Boissiere, C.; Nicole, L.; Sanchez, C.; Le Floch, P.; Mezailles, N. *Chem. Mater.* **2010**, *22*, 1340.

(6) Bala, T.; Gunning, R. D.; Venkatesan, M.; Godsell, J. F.; Roy, S.; Ryan, K. M. *Nanotechnology* **2009**, *20*, 415603.

(7) Xia, Y.; Xiong, Y. J.; Lim, B.; Skrabalak, S. E. *Angew. Chem., Int. Ed.* **2009**, *48*, 60.

(8) Bratlie, K. M.; Lee, H.; Komvopoulos, K.; Yang, P.; Somorjai, G. A. *Nano Lett.* **2007**, *7*, 3097.

(9) Sun, S. H.; Murray, C. B.; Weller, D.; Folks, L.; Moser, A. *Science* **2000**, *287*, 1989.

(10) Xiong, Y. J.; Cai, H. G.; Wiley, B. J.; Wang, J. G.; Kim, M. J.; Xia, Y. N. *J. Am. Chem. Soc.* **2007**, *129*, 3665.

(11) Zhang, Y. W.; Grass, M. E.; Kuhn, J. N.; Tao, F.; Habas, S. E.; Huang, W. Y.; Yang, P. D.; Somorjai, G. A. *J. Am. Chem. Soc.* **2008**, *130*, 5868.

(12) Dumestre, F.; Chaudret, B.; Amiens, C.; Renaud, P.; Fejes, P. *Science* **2004**, *303*, 821.

(13) Ren, J. T.; Tilley, R. D. *J. Am. Chem. Soc.* **2007**, *129*, 3287.

(14) Kang, Y. J.; Ye, X. C.; Murray, C. B. *Angew. Chem., Int. Ed.* **2010**, *49*, 6156.

(15) Zhang, J.; Fang, J. Y. *J. Am. Chem. Soc.* **2009**, *131*, 18543.

(16) Wu, J.; Gross, A.; Yang, H. *Nano Lett.* **2011**, *11*, 798.

(17) Wu, B.; Zheng, N.; Fu, G. *Chem. Commun.* **2011**, *47*, 1039.

(18) Cordente, N.; Respaud, M.; Senocq, F.; Casanove, M. J.; Amiens, C.; Chaudret, B. *Nano Lett.* **2001**, *1*, 565.

(19) Bradley, J. S.; Tesche, B.; Busser, W.; Maase, M.; Reetz, M. T. *J. Am. Chem. Soc.* **2000**, *122*, 4631.

(20) Leng, Y. H.; Zhang, Y. H.; Liu, T.; Suzuki, M.; Li, X. G. *Nanotechnology* **2006**, *17*, 1797.

(21) Watt, J.; Young, N.; Haigh, S.; Kirkland, A.; Tilley, R. D. *Adv. Mater.* **2009**, *21*, 2288.

(22) Watt, J.; Cheong, S.; Toney, M. F.; Ingham, B.; Cookson, J.; Bishop, P. T.; Tilley, R. D. *ACS Nano* **2010**, *4*, 396.

(23) Cheong, S.; Watt, J.; Ingham, B.; Toney, M. F.; Tilley, R. D. *J. Am. Chem. Soc.* **2009**, *131*, 14590.

(24) Cheong, S.; Ferguson, P.; Feindel, K. W.; Hermans, I. F.; Callaghan, P. T.; Meyer, C.; Slocombe, A.; Su, C.-H.; Cheng, F.-Y.; Yeh, C.-S.; Ingham, B.; Toney, M. F.; Tilley, R. D. *Angew. Chem., Int. Ed.* **2011**, *50*, 4206.

(25) Herman, D. A. J.; Ferguson, P.; Cheong, S.; Hermans, I. F.; Ruck, B. J.; Allan, K. M.; Prabakar, S.; Spencer, J. L.; Lendrum, C. D.; Tilley, R. D. *Chem. Commun.* **2011**, *47*, 9221.

(26) Bhatia, B.; Sholl, D. S. *J. Chem. Phys.* **2005**, *122*, 204707.

(27) O'Handley, R. C. *Modern Magnetic Materials: Principles and Applications*; Wiley: New York, 2000.

(28) Nogues, J.; Schuller, I. K. *J. Magn. Magn. Mater.* **1999**, *192*, 203.

(29) Johnston-Peck, A. C.; Wang, J.; Tracy, J. B. *ACS Nano* **2009**, *3*, 1077.